Electrospun PMMA polymer blend nanofibrous membrane: electrospinability, surface morphology and mechanical response

Jacky Jia Li Lee, Andri Andriyana, Bee Chin Ang, Bertrand Huneau, Erwan Verron

Electrospun PMMA Polymer Blend Nanofibrous Membrane: Electrospinability, Surface Morphology and Mechanical Response

Jacky Jia Li Lee[1,a], Andri Andriyana[1*,b], Bee Chin Ang[2,c], Bertrand Huneau[3,d], Erwan Verron[3,e]

[1]Centre of Advanced Materials,
Department of Mechanical Engineering,
University of Malaya,
50603 Kuala Lumpur, Malaysia.
[2]Centre of Advanced Materials,
Department of Chemical Engineering,
University of Malaya,
50603 Kuala Lumpur, Malaysia.
[3]École Centrale de Nantes,
GeM,
UMR CNRS 6183, BP92101,
44321 Nantes cedex 3, France.
[a] jacky_ljl@siswa.um.edu.my, [b] andri.andriyana@um.edu.my, [c] amelynang@um.edu.my,
[d] bertrand.huneau@ec-nantes.fr, [e] erwan.verron@ec-nantes.fr

* Corresponding Author.

Abstract: The present work focuses on the electrospinning ability, the evaluation of resulting surface morphology and mechanical response of PMMA polymer blend nanofibrous membranes. For this purpose, electrospinning ability of PMMA polymer blend is firstly investigated by exploring various set of electrospinning parameters. From the evaluation of surface morphology of the resulting electrospun membranes, the optimum parameters are identified. Using these optimum parameters, tensile specimens are subsequently produced. Three deformation modes are considered: monotonic tensile test, cyclic test with increasing maximum strain and cyclic-relaxation test. Morphological analysis shows that the optimized tensile specimens are initially isotropic on the plane. The mechanical test results highlight the strong inelastic responses of the materials, which include inelastic strain and time-dependent behavior characterized by stress relaxation. Finally, in-situ tensile test outcomes suggest that strain-induced fiber re-orientation took place.

1.0 Introduction

The advancement in technologies led to the extensive researches in the submicron to nano-scaled materials because nano-scaled materials have far superior properties when compared to their bulk form. Among all the nano-scaled materials, nanofibrous membranes are one of the materials that are explored due to their magnificent property of surface area to weight ratio. This property has motivated the use of nanofibrous membranes in applications such as filtration, biomedical applications, sensors and clothings [1-9].

Electrospinning is a versatile fabrication technique for producing nanofibrous membranes. The access to manipulate easily the membrane morphology through proper adjustment of different relevant processing parameters has made electrospinning to be widely used. A large variety of polymers can be used to produce nanofibrous membranes including polyethylene oxide (PEO), polyvinyl alcohol (PVA), polyacrylonitrile (PAN), polyvinylidene fluoride (PVDF) and poly(methyl methacrylate) (PMMA) along with different kind of fillers [9-19]. PMMA was chosen in this study due to its mechanical properties [20, 21] and its biocompactibility [22]. In view of further improving the physical and mechanical properties of the nanofibrous membranes, PMMA polymer blend, which is composed of high and low molecular weight PMMA, was adopted in this research.

From a number of works in the literature dealing with electrospinning parameters, it appears that their effect depends on the type of polymer used [9, 13, 23, 24]. Since there is no study available on the role of electrospinning parameters on the morphology of PMMA polymer blend nanofibrous membrane, it is essential to explore this effect in such materials.

In a number of works, simple monotonic tensile tests on single nanofiber were conducted to obtain the mechanical properties [25, 26]. Alternatively, the mechanical properties of

nanofibrous membranes were probed using atomic force microscopy (AFM) [27, 28]. Moreover, the effect of different strain rates [29] and different temperatures [30] on the mechanical properties of the nanofibrous membranes were recently investigated. However, to the best of our knowledge, only basic mechanical properties such as Young's modulus, tensile strength and strain at fracture were commonly investigated. Indeed, only few studies focused on the mechanical behavior of non-aligned nanofibrous membrane under complex loading histories and the corresponding micromechanism deformation of nanofibrous membranes under loading [23].

In this work, a polymer blend of high molecular weight poly(methyl methacrylate) (PMMA) (M_w ~996,000 g/mol) and low molecular weight PMMA (M_w~120,000 g/mol) was considered to fabricate nanofibrous membrane using electrospinning technique. The electrospinability and also the parameters for producing the best nanofibrous membrane (smallest fiber diameters and least beads) was also determined in this study.

In addition, the mechanical properties and responses of the nanofibrous membranes produced using optimum parameters were determined. Three types of mechanical tests were considered: monotonic tensile, cyclic loading with increasing maximum strain and cyclic loading interrupted with several relaxation segments. Moreover, in-situ tensile test in SEM was also carried out. It is to note that, the mentioned in-situ tenstile test in SEM has never been carried out before to study the micromechanism deformation of the nanofibrous membranes and the re-orientation of the fibers upon deformation.

2.0 Experiemental

2.1 Materials

PMMA polymer of average molecular weight of 996,000 g/mol (referred to as high molecular weight PMMA) and 120,000 g/mol (referred to as low molecular weight PMMA) were considered. Moreover, N,N-dimethylformamide (DMF) was used as the solvent. All materials were obtained from Sigma-Aldrich.

2.2 Experimental Design

The parameters for all samples prepared are shown in **Table 1**. Weight percentage was calculated by dividing the weight of PMMA with the weight of the total solution (DMF+PMMA). All solutions were prepared one day before electrospinning to ensure that PMMA was fully dissolved in DMF. During the stirring process, reflux process was used to prevent DMF from evaporating out from the flasks. After PMMA had been completely dissolved, the polymer solution was then electrospun onto aluminium foil which was attached on a stationary stainless steel plate. The setup for electrospinning is shown in **Figure 1**. The setup for electrospinning is shown in **Figure 1**.

2.3 Characterization

The surface morphology of the samples was obtained by using the SEM Phenom ProX. All nanofibrous membranes were coated with a thin layer of platinum using the platinum coater. The mean diameters of the nanofibers were obtained by calculating the mean value of 100 readings obtained by using the software ImageJ.

High molecular weight PMMA, low molecular weight PMMA, PMMA polymer blend film as well as the chosen PMMA polymer blend nanofibrous membrane were sent for thermogravimetric analysis (TGA) to investigate their thermal properties.

2.4 Mechanical Tests

Mechanical tests were carried out using Shimadzu AGS-X Series Universal Tensile Testing Machine equipped with 50N load cell at strain rate of 5.5×10^{-4} sec^{-1}. 2 cm x 6 cm PMMA polymer blend nanofibrous membranes were cut and used for the mechanical tests. Before the mechanical tests were conducted, the thickness of each specimen was measured using the Mitutoyo ABSOLUTE Digimatic Caliper with accuracy of 0.01 mm. The gauge length was fixed at 3 cm.

Three types of mechanical tests were conducted: monotonic tensile, cyclic loading with increasing maximum strain and cyclic loading interrupted with several relaxation segments (referred to as cyclic-relaxation in the rest of the paper). For monotonic tensile loading, the selected PMMA polymer blend nanofibrous specimen was stretched until fracture. Meanwhile for cyclic loading test, the specimen was initially subjected to a maximum strain of 1% before it is increased by 1% for each subsequent cycle until 9% maximum strain. The specimen was

then continued to be stretched until fracture. It is to note that in each cycle, the specimen was unloaded to zero stress (zero force) instead of zero strain in order to avoid specimen buckling. The cyclic loading profile is shown in **Figure 2**(a).

For cyclic-relaxation, the specimen was stretched up to 2% strain and held for 15 minutes at constant strain. The tensile specimen was then stretched further to 4% strain and held for 15 minutes before it is re-stretched to a maximum strain of 6%. Afterwards, the specimen was unloaded and similar relaxation segments were introduced during the unloading at the strain levels of 4% and 2%. Similarly to uploading, each relaxation is conducted for the duration of 15 minutes. The profile for cyclic-relaxation test is shown in Figure 2(b). It is to note that this loading sequence is inspired from the works of Lion (1996) [31] and Bergström and Boyce (1998) [32].

2.5 In-situ Tensile Test in SEM and Orientation Tensor

In order to observe the effect of mechanical loading on the orientations of the fibers, in-situ tensile test in SEM was carried out. For this purpose, a Deben tensile stage was used. The SEM used in this section is JEOL JSM-6060LV. The tensile stage attached into the SEM is shown in **Figure 3**.

The average orientations of the fibers at initial and stretched states were then described by the use of orientation tensor, thereby allowing the study of strain-induced fiber re-orientation in the materials.

40 images were taken for each maximum strain. The orientation distributions were then taken using OrientationJ, a plugin for ImageJ [33]. The distributions were then normalized with respect to total amount of fibers to obtain the normalized probability density of the orientations of fibers.

The method to obtain the orientation tensor of the fibers have been developed by Advani and Tucker [34]. According to their study, in order to properly describe the vector of the fibers, **p**, two *Eulerian* angles, $\alpha \in [0,\pi]$ and $\beta \in [0,2\pi]$ are needed, as shown in **Figure 4**.

In summary, the components of the vector **p** of the fibers are:

$$p_1 = \sin\alpha \cos\beta \quad (1)$$

$$p_2 = \sin\alpha \sin\beta \quad (2)$$

$$p_3 = \cos\alpha \quad (3)$$

where $(p_i)_{i=1,2,3}$ are the components of vector **p** in the axis of $(e_i)_{i=1,2,3}$. Thus,

$$\mathbf{p} = \sin\alpha \cos\beta\, \boldsymbol{e_1} + \sin\alpha \sin\beta\, \boldsymbol{e_2} + \cos\alpha\, \boldsymbol{e_3} \quad (4)$$

The tensor of the orientation can be expressed in terms of 3x3 matrix:

$$\mathbf{A}_0 = \sum_{i,j=1}^{3} A_{0ij}\, \mathbf{e}_\mathrm{i} \times \mathbf{e}_\mathrm{j} \quad (5)$$

which means that once the normalized probability density of the orientation of fibers ρ has been obtained, the tensor of orientation $\mathbf{A}_0$ can be obtained. The orientation tensor $\mathbf{A}_0$ can be represented as:

$$\mathbf{A}_0 = \begin{bmatrix} A_{011} & A_{012} & A_{013} \\ A_{021} & A_{022} & A_{023} \\ A_{031} & A_{032} & A_{033} \end{bmatrix} \quad (6)$$

However, due to the nanofibrous membrane being a planar-like structure, the orientation tensor $\mathbf{A}_0$ can be reduced to

$$\mathbf{A}_0 = \begin{bmatrix} A_{011} & A_{012} & 0 \\ A_{021} & A_{022} & 0 \\ 0 & 0 & 0 \end{bmatrix} \quad (7)$$

3. Results and Discussion

3.1 Electrospinability

As shown in Table 1, various parameters have been optimized in order to produce PMMA polymer blend nanofibrous membranes which are suitable for filtration application, i.e. possess certain strength to withstand water pressure and contain high fiber amount to enhance filtration capabilities. Each assigned letter indicated a change in one of the parameters.

Before the electrospinning of the polymer blends, high M_w PMMA and low M_w PMMA have been electrospun separately to determine their electrospinability and physical properties. Based on the research conducted by Mohammad Khanlou et al. (2015),[35] it requires at least 15 wt% and a maximum of 25 wt% of low M_w PMMA to produce nanofibrous membranes.

Meanwhile for high M_w PMMA, it requires a minimum of 3 wt% and a maximum of 7 wt% of high M_w PMMA to successfully produce nanofibrous membranes.

Through physical inspection, it was found that the nanofibrous membrane produced from low Mw PMMA had a higher amount of fibers formed and the resulting membrane was thicker. This observation can be related to the higher polymer content in the solution. Indeed, the higher polymer content promotes higher polymer chain entanglement which leads to a thicker membrane [36]. At the macroscopic level, the membrane's surface appeared to be fibrous as shown in **Figure 5**. This observation is similar and analogy to the structure of polymer crystalline spherulite, where amorphous regions (macroscopic fibril surface of electrospun membrane) are found outside the crystalline lamellae (electrospun membrane).

On the other hand, for the same volume of polymer solution and the same electrospinning duration, nanofibrous membrane produced from high Mw PMMA was found to be thinner. The lower amount of polymer content used for high Mw PMMA led to lower polymer entanglements during electrospinning and thinner electrospun membrane [36]. The nanofibrous membrane produced was brittle but the surface of the nanofibrous membrane produced was smooth as shown in **Figure 6**.

For the electrospinability of various polymer concentrations, when Samples H1-H4 were compared, the high M_w PMMA concentration was varied while the low M_w PMMA concentration and electrospinning parameters were fixed at 15 wt%. The results showed that only Samples H1 and H2 could be electrospun. The electrospinning parameters for Samples H3 and H4 were then modified and labeled as Samples P1-P10 as shown in Table 1 for further analysis on the electrospinability of the polymer concentrations. However, the PMMA polymer blend nanofibrous membrane still cannot be electrospun for high M_w PMMA concentration of

4 wt% and 5 wt% paired with low M_w PMMA concentration of 15 wt% regardless of varying electrospinning parameters.

The low M_w PMMA concentrations were then varied accordingly with high M_w PMMA concentrations as shown for Samples A1-A4, B1-B4 and C1-C4. From these samples, only Samples A3, A4, B3, B4, C1 and C2 can be electrospun. Therefore, it is found that the minimum requirement for electrospinning PMMA polymer blend is to have either ≥15 wt% low M_w PMMA and <4 wt% high M_w PMMA or ≥4 wt% high M_w PMMA and <15 wt% low M_w PMMA. Higher polymer content of the PMMA polymer blend led to highly viscous polymer solution which impedes the ability to control and maintain the flow of polymer solution to the tip of the needle during electrospinning [37].

After electrospun various polymer blend concentrations, it was also noticed that the physical properties of the nanofibrous membranes were dependent on the dominant polymer type. Polymer blend with higher high M_w PMMA concentration tend to form more brittle nanofibrous membranes while polymer blend with higher low M_w PMMA concentration tend to form fibrous nanofibrous membranes.

In the direction of overcoming the undesirable properties of brittleness, fibrous surface and thickness of nanofibrous membrane, the optimum polymer blend concentration was selected through physical inspection: 4 wt% high M_w PMMA and 8 wt% low M_w PMMA. Various electrospinning parameters were manipulated for this polymer blend concentration to further improve the surface morphology of the nanofibrous membranes.

3.2 Surface Morphology of Electrospun Nanofibrous Membranes

The concentration of the polymer blend was fixed at 4 wt% high M_w PMMA and 8 wt% low M_w PMMA as the physical properties favors the filtration application as well as for studying the mechanical properties of the nanofibrous membranes. The surface morphology of the nanofibrous membranes were obtained through SEM. In order to study precisely the effect of the main processing parameters of electrospinning on the surface morphology of the nanofibrous membranes, one of the processing parameters was altered while the other processing parameters remained constant. The effects of the processing parameters are discussed as follows.

3.2.1 Feed Rate

In this study, the feed rates used were 0.5 ml/h, 1.0 ml/h and 2.0 ml/h and were labeled as F1, F2 and F3 respectively. The SEM images of the three samples as well as the graph comparing the average fibers diameter of the nanofibrous membranes are shown in **Figure 7**.

As seen from the SEM images in Figure 7, there are no beads formed in all three samples. This is because the feed rates used in this study are adequate to provide stable flow of the solution during electrospinning and the electrical force of the electrospinning is able to overcome the surface tension of the polymer blend. These observation and deduction are also seen and explained in other polymer solutions [38, 39].

Meanwhile, the average fibers diameters of the nanofibrous membranes for sample F1, F2 and F3 are shown in Figure 7 (d). At 0.5 ml/h, the average fibers diameter is 729 nm ± 18 nm and this value decreases to 661 nm ± 11 nm when the feed rate is increased to 1.0 ml/h.

However, the value increases to 782 nm ± 13 nm when the feed rate is further increased to 2.0 ml/h. In most researches did by other researchers on polymer solutions, they observed an increase in fiber diameter with increasing feed rate [11, 35, 40].

However, in this study, the lowest feed rate causes an increase in the fiber diameter. This is mainly due to not achieving the minimum flow rate mandatory for electrospinning [41]. The low flow rate caused the solution to be pulled to the collector during electrospinning within the needle, causing the flow of the solution to be unstable, which led to the larger fiber diameter. On the other hand, the fibers diameter increases with high flow rate because with high flow rate, more polymer solution are pulled to the collector, thus causing the solvent in the solution to be more difficult to evaporate, leading to the increase in fibers diameter [42].

3.2.2 Supply Voltage

The effect of the supply voltage on the surface morphology of the nanofibrous membranes are studied by comparing samples V1, F2 and V2, which are electrospun at 10 kV, 15 kV and 20 kV respectively. The SEM images of the three samples as well as graph comparing the average fiber diameters of the three samples are shown in **Figure 8**.

There are tiny, little beads formed in Sample V1 while for Sample F2 and V2, no bead is observed. Beads are formed in Sample V1, which is produced using supply voltage of 13 kV because the lower supply voltage does not provide sufficient electrical force to stretch the fibers and eliminate the beads during electrospinning [42]. Meanwhile, beads are not formed in Sample F2 and V2 because the polymer concentration used and the electrospinning parameters are within the correct range to prevent beads formation.

The average fibers diameter, are 794 nm ± 14 nm, 661 nm ± 11 nm and 694 nm ± 9 nm for applied voltage of 13 kV, 15 kV and 20 kV respectively. The average fibers diameter decreases

when the supply voltage is increased from 13 kV to 15 kV because the increase supply voltage increases the electrical force, which aids in overcoming the surface tension of the polymer solution as well as the "pulling force" to elongate the fibers upon reaching the collector. This observation is also found in research did by Zhang, Wang [13] on polyacrylonitrile (PAN). On the contrary, the average fibers diameter increases when the supply voltage is increased from 15 kV to 20 kV. In this case, the high supply voltage causes the discontinuity of the polymer solution flowing out from the needle, as well as the high electrical force causes the fibers to reached the collector faster, reducing the time of stretching of the fibers [42].

3.2.3 Working Distance

Working distance of electrospinning is also studied in this research. The distances studied are labeled as D1, F2 and D2, which has a working distance of 10 cm, 15 cm and 20 cm respectively. The SEM images of three samples as well as the graph comparing the average fiber diameter of the three samples are shown in **Figure 9**.

No beads are observed in all three samples. This signified that the working distances used in this study provide sufficient time for the polymer solution to split and elongate, thus eliminating the beads formation. This phenomenon is also explained by Buchko et al. [43].

On the other hand, the average fibers diameters of the three samples obtained are 769 nm ± 14 nm, 661 nm ± 11 nm and 751 nm ± 11 nm respectively. The average fibers diameters decreased with increasing working distance from 10 cm to 15 cm. The increase in working distance provides longer time for the polymer solution to split and elongate during electrospinning before reaching the collector. However, the average fiber diameter is found to increase when the working distance is increased from 15 cm to 20 cm. Different studies on effect of working distance has been made by other researchers, but results obtained were

different [12, 42, 44]. It can be believed that the effect of working distance varied with other factors such as type of polymer, supply voltage and type of solvent. In order to study the effect of the working distance on the surface morphology of the nanofibrous membrane, the supply voltage was kept constant at 15 kV. With the supply voltage fixed at 15 kV, even though the increase in working distance would provide longer time for splitting and elongation, the electrical force would decrease. When the working distance is increased to 20 cm, the effect of lower electrical force per distance is predominant than the longer polymer solution travelling duration, thus leading to an increase in the average fiber diameter of the nanofibrous membrane.

3.2.4 Gauge Size

The effect of gauge size on the surface morphology of the nanofibrous membrane is also studied. The three samples used for comparisons are G1, G2 and F2, with the gauge size of 0.6 mm, 0.8 mm and 1.1 mm respectively. The SEM images as well as the graph comparing the average fiber diameter of the three samples are shown in **Figure 10**.

From Figure 10, there are no beads found in all three samples. This signifies that the gauge sizes used do not affect the beads formation of the nanofibrous membrane.

Meanwhile the average fibers diameters obtained for the samples are 672 nm ± 10 nm, 657 nm ± 9 nm and 661 nm ± 11 nm respectively. The minor difference in the average fiber diameter is caused by the error obtaining the fibers diameter when using ImageJ, but this error had been minimized as 100 readings were taken to obtain the average fibers diameter. This showed that the gauge size did not affect the beads formation as well as the surface morphology of the nanofibrous membrane.

However, during the electrospinning process, the use of smaller gauge size tends to clog the flow of polymer solution. Therefore, in the production of nanofibrous membrane for mechanical tests, 1.1 mm gauge is used to ease the electrospinning process.

3.3 Thermal Analysis

High M_w PMMA, low M_w PMMA, PMMA polymer blend film and PMMA polymer blend nanofibrous membrane (F2) were sent for thermal analysis. PMMA polymer blend film was prepared by casting the PMMA polymer blend solution in a Petri dish. **Figure 11** shows the graph of weight percentage against temperature for all four samples.

From Figure 11, all four samples start to decompose at a higher temperature than the minimum thermal decomposition (528°C) recorded by Beyler and Hirschler [45]. Low Mw PMMA, high Mw PMMA and PMMA blend film showed early stages of decomposition at 720 °C, 660 °C and 650 °C respectively. PMMA blend fiber on the other hand, starts to decompose at temperature of 750 °C. The increase in the decomposition temperature is presumed to be caused by the increase in the crystallinity after electrospinning of PMMA polymer blend. During the electrospinning process, the polymer will tend to align in long chain order and increase the crystallinity and hence increase the thermal stability.

3.4 Mechanical Tests

Based on the results discussed in Section 3.2, the best nanofibrous membrane is Sample F2, which has the smallest average fibers diameter (661nm ± 11 nm) without any observable beads.

This optimized nanofibrous membrane can be produced by using 4 wt% high M_w PMMA and 8 wt% low M_w PMMA along with the following electrospinning parameters: supply voltage of 15 kV, feed rate of 1.0 ml/h, working distance of 15 cm and gauge size of 1.1 mm. Therefore, this set of parameters is used to produce nanofibrous membranes for mechanical tests.

The following mechanical tests were carried out to study the mechanical responses of the nanofibrous membranes: monotonic tensile, cyclic loading and cyclic-relaxation. The results obtained are discussed as follows.

3.4.1 Monotonic Tensile

Monotonic tensile was carried out at a strain rate of 5.5×10^{-4} sec^{-1}. Two samples were tested for monotonic tensile test. **Figure 12** (a) shows the stress-strain curve obtained from both samples in monotonic tensile loading. The stress-strain curves obtained from both samples are relatively similar.

From the stress-strain curves obtained from both samples in Figure 12, the engineering stress increased until the sample reached maximum stress. As the applied strain was further increased, the stress started to decrease. Furthermore, it appeared that the stress decreased at a lower rate as the sample was further strained until it underwent fracture at approximately 27% strain.

From the stress-strain curves of the two samples in Figure 12, the average Young's Modulus, yield strength and stress at fracture are found to be 11.65 MPa, 145 kPa and 24 kPa respectively. The Young's Modulus was calculated by calculating the gradient of the elastic region from the stress-strain curve. The yield point was determined through 0.2% offset method.

In electrospun nanofibrous membranes, Wong et al. [23] suggested the existence of two competing phenomena related to topology change: deformation induced fiber re-orientation and deformation-induced inter-fiber bond damage. The phenomena of realignment of fibers and permanent damage were also observed by Ridruejo et al. [29]. The realignment of the fibers were observed and discussed in Section 3.4.4.

At around 1.5% strain onwards, it was found that the stress-strain curves in Figure 12 (a) obtained were fluctuating. While the possible reason for this fluctuation remains unclear, it could be possibly due to the fibers in the nanofibrous membrane escaping or hooking onto the fiber membrane itself, causing the decrease or increase in the stress obtained. This phenomenon can be observed during tensile test under optical microscope and in-situ tensile test in SEM (see section 3.4.4).

Figure 12 (b) shows the stress-strain curve of PMMA film as comparison [46]. It was noticed that both bulk PMMA and PMMA polymer blend nanofibrous membrane showed qualitative similar stress-strain curve. In bulk PMMA, the general stress-strain characteristics is often described by cold drawing, where two competing phenomena take place: necking and deformation-induced polymeric chain re-alignment [47]. In electrospun nanofibrous membranes, Wong et al. [23] suggested the existence of two competing phenomena related to topology change: deformation induced fiber re-orientation and deformation-induced inter-fiber bond damage. The phenomena of realignment of fibers and permanent damage were also observed by Ridruejo et al. [29]. The realignment of the fibers were observed and discussed in Section 3.4.4.

3.4.2 Cyclic Loading

In cyclic loading, the nanofibrous membrane was subjected to uploading and unloading with increasing maximum strain until the nanofibrous membrane fractured. The test was carried out to determine the behavior of inelastic deformation as well as the evolution of the elastic modulus of the nanofibrous membranes. The results obtained from cyclic loading were shown in **Figure 13**.

From Figure 13, beyond a certain level of strain, the nanofibrous membrane did not return to its original position after unloading, i.e. inelastic deformation occurred in the nanofibrous membrane. To further understand the behavior of the inelastic deformations of the nanofibrous membrane, a graph of inelastic strain ratio, $\varepsilon_p/\varepsilon_{max}$ against maximum strain ε_{max} was plotted. The inelastic strain ratio is calculated by dividing the inelastic strain with the corresponding maximum strain. The graph of inelastic strain ratio against maximum strain is shown in **Figure 14** (a).

As seen in Figure 14 (a), the nanofibrous membrane experienced high amount of inelastic deformation before fracture. The inelastic deformation experienced by the nanofibrous membrane also increased with increasing maximum strain in a non-linear way.

By calculating the Young's Modulus of the nanofibrous membrane at each uploading curve, the graph of Young's Modulus against maximum strain was plotted and shown in Figure 14 (b).

Figure 14 (b) illustrates the changes of stiffness of the nanofibrous membrane with respect to the changes in maximum strain. The curve showed an increasing trend at the initial stages, then the Young's Modulus decreased at 2% to 4% maximum strain. The Young's Modulus then remained nearly constant from 4% maximum strain until fracture. The initial increase in the Young's Modulus could be attributed to the realignment of the fibers with deformation, which

caused an increase in the stiffness of the nanofibrous membrane. On the other hand, the following decrease in Young's Modulus after 2% strain might be caused by the permanent broken of physical junctions between the fibers. At early stages, damage of fibers also occurred. However, the contribution of the damage on the stiffness is lower compared to the realignment of the fibers. As mentioned by Ridruejo et al. [29], the damage of fibers occurred at the very low maximum strains, which leads to further fiber rearrangement. After 2% strain, the damage in the fibers appeared to become predominant, thus causing the decrease in the stiffness at 4% maximum strain.

3.4.3 Cyclic-relaxation Test

Cyclic-relaxation test was carried out to study the material's behavior through the change in stress values when the material is held at constant strain over a specific duration. From the stress-strain curve obtained after performing the stress-relaxation test, the first and second relaxation showed similar trend, which drop rapidly and eventually achieve equilibrium at the end of the curve. In order to compare the rate of relaxation, both first and second relaxations were normalized by dividing the value of stress with their first value of stress. **Figure 15** shows the normalized stress versus time at the first and second relaxation parts.

From Figure 15, the two normalized stress curve from first relaxation and second relaxation coincide, thus at both relaxations, the nanofibrous membrane achieved equilibrium at the same rate. This shows that the nanofibrous membrane exhibits linear viscoelastic behavior where the rate of relaxation is independent of strain level.

3.3.4 In-situ Tensile Testing in SEM

In-situ tensile test in SEM was also carried out on the nanofibrous membrane. The main purpose of this in-situ tensile test is to study the evolution of fiber orientation as the nanofibrous membrane deforms. From the SEM images shown in **Figure 16**, fibers in the nanofibrous membranes had been reoriented after subjected to tensile loading.

Figure 17 shows the graph of normalized distribution of nanofibrous membranes stretched at different maximum strain against fiber orientations.

The 0° angle corresponds to a direction parallel to the direction of tensile force. As seen in Figure 16, before the tensile test was carried out, the nanofibrous membrane was essentially isotropic on the plane, having fibers distributed randomly in all directions. However, after the nanofibrous membrane was stretched to 10% strain, the fibers started to realign themselves parallel to the direction of tensile force. As the nanofibrous membrane was further stretched to higher strain levels, the fibers kept on realigning themselves parallel to the direction of tensile force. **Figure 18** shows the illustrations of the fibers orientation at different strain levels.

The results were then further analyzed in the form of orientation tensors. Through the orientation tensors, the rate of realignment of the fibers can be determined. The orientation tensors were calculated based on the equations as discussed in Section 2.5. In order to determine the rate of re-orientation of the fibers in the nanofibrous membrane, the value of A_{011} in the orientation tensor against respective stretch is required. **Figure 19** shows the value of A_{011} of orientation tensor against stretch of the nanofibrous membrane.

Based on Figure 19, the value of A_{011} started off at 0.5, which signified that the nanofibrous membrane was initially isotropic on the plane, having fibers randomly distributed in all directions on the plane of the nanofibrous membrane. Once the fibers were further stretched to

maximum strain of 20%, the value of A_{011} increased to maximum of 0.75. The value of A_{011} remained the same despite being further stretched to 30% maximum strain.

Finally, it is to note that due to the lengthy procedure of in-situ tensile test in SEM and as seen in the relaxation test in Section 3.4.3, relaxation had already taken place in the SEM while the orientations of the fibers were taken. Consequently, the obtained orientations correspond to the equilibrium state of the fibers. Further improvement of in-situ tensile test should be introduced in order to access the fiber orientation at any given applied strain.

4. CONCLUSION

PMMA polymer blend nanofibrous membranes were succesfully produced through electrospinning. Different PMMA blend concentrations had been tested to check on the electrospinability as well as the physical properties of the nanofibrous membranes produced. Through physical inspections, the optimum polymer blend concentration that was able to produce nanofibrous membranes suitable for mechanical tests was 4 wt% high M_w PMMA and 8 wt% low M_w PMMA.

The optimum parameters to electrospin the PMMA polymer blend nanofibrous membrane are 4 wt% high M_w PMMA, 8 wt% low M_w PMMA, 1.0 ml/h feed rate, 15 kV supply voltage, 15 cm working distance and 1.1mm gauge size, which are able to obtain beadless non-woven nanofibrous membrane with average fibers diameter of 661 ± 11 nm.

Thermogravimetric analysis showed an increase in thermal stability with the electrospinning of PMMA polymer blend nanofibrous membrane as compared to its powder form and normal film casting.

Through the mechanical tests, the nanofibrous membrane has a Young's Modulus of 11.65 MPa. The average yield strength is 145 kPa while the average stress at fracture is 24 kPa. The general stress-strain characteristics of the membrane could be related to either instricsic cold draws or interaction between fiber reorientation and inter-fiber damage. Cyclic loading showed that the material underwent high inelastic deformation before complete rupture. Stress-relaxation test showed that the nanofibrous membranes exhibit linear viscoelastic response. In-situ test showed that the nanofibrous membrane realigned themselves parallel to the direction of tensile force with increasing strain.

ACKNOWLEDGEMENT

The authors greatly appreciate the financial support from University of Malaya under the University of Malaya Research Grant (UMRG) fund (Grant No. RP034C-15AET and RP034E-15AET), Fundamental Research Grant Scheme (FRGS) fund (Grant No. FP048-2013B), Ministry of Higher Education Malaysia through High Impact Research Grant (Grant No. D000008-16001) and from Embassy of France in Malaysia.

Keywords: PMMA, surface morphology, isotropic nanofibrous membrane, mechanical properties, electrospinning

REFERENCES

1. Ding, B., et al., *Gas sensors based on electrospun nanofibers.* Sensors, 2009. **9**(3): p. 1609-1624.
2. Heikkilä, P., et al., *Electrospinning of polyamides with different chain compositions for filtration application.* Polymer Engineering & Science, 2008. **48**(6): p. 1168-1176.
3. Huang, Z.-M., et al., *A review on polymer nanofibers by electrospinning and their applications in nanocomposites.* Composites Science and Technology, 2003. **63**(15): p. 2223-2253.
4. Khil, M.-S., et al., *Electrospun nanofibrous polyurethane membrane as wound dressing.* Journal of Biomedical Materials Research Part B: Applied Biomaterials, 2003. **67B**(2): p. 675-679.
5. Talebian, S., et al., *Chitosan (PEO)/bioactive glass hybrid nanofibers for bone tissue engineering.* RSC Adv., 2014. **4**(90): p. 49144-49152.
6. Unnithan, A.R., et al., *Wound-dressing materials with antibacterial activity from electrospun polyurethane–dextran nanofiber mats containing ciprofloxacin HCl.* Carbohydrate Polymers, 2012. **90**(4): p. 1786-1793.
7. Wang, X., et al., *Electrospun Nanofibrous Membranes for Highly Sensitive Optical Sensors.* Nano Letters, 2002. **2**(11): p. 1273-1275.
8. Yu, D.-G., et al., *PVP nanofibers prepared using co-axial electrospinning with salt solution as sheath fluid.* Materials Letters, 2012. **67**(1): p. 78-80.
9. Zhou, W., et al., *Ultra-filtration membranes based on electrospun poly(vinylidene fluoride) (PVDF) fibrous composite membrane scaffolds.* RSC Advances, 2013. **3**(29): p. 11614-11620.
10. Cheng, L., et al., *NaF-loaded core–shell PAN–PMMA nanofibers as reinforcements for Bis-GMA/TEGDMA restorative resins.* Materials Science and Engineering: C, 2014. **34**: p. 262-269.
11. Doshi, J. and D.H. Reneker. *Electrospinning process and applications of electrospun fibers*. in *Industry Applications Society Annual Meeting, 1993., Conference Record of the 1993 IEEE*. 1993.
12. Lee, J.S., et al., *Role of molecular weight of atactic poly (vinyl alcohol)(PVA) in the structure and properties of PVA nanofabric prepared by electrospinning.* Journal of Applied Polymer Science, 2004. **93**(4): p. 1638-1646.
13. Zhang, X., et al., *The Morphology of the Hollow PAN Fibers through Electrospinning.* AASRI Procedia, 2012. **3**: p. 236-241.
14. Tao, J. and S. Shivkumar, *Molecular weight dependent structural regimes during the electrospinning of PVA.* Materials Letters, 2007. **61**(11–12): p. 2325-2328.
15. Islam, M.S., et al. *Fabrication and Characterization of Poly (Vinyl Alcohol)/Chitosan Blend Electrospun Nanofibrous Membrane*. in *Key Engineering Materials*. 2016. Trans Tech Publ.
16. Wong, D., et al. *Surface Morphology Analysis and Mechanical Characterization of Electrospun Nanofibrous Structure*. in *Key Engineering Materials*. 2016. Trans Tech Publ.
17. Lee, J.J.L., et al., *Fabrication of PMMA/zeolite nanofibrous membrane through electrospinning and its adsorption behavior.* Journal of Applied Polymer Science, 2017. **134**(6).
18. Li, L., et al., *Hierarchically structured PMMA fibers fabricated by electrospinning.* RSC Advances, 2014. **4**(95): p. 52973-52985.

19. Bae, H.-S., et al., *Fabrication of highly porous PMMA electrospun fibers and their application in the removal of phenol and iodine.* Journal of Polymer Research, 2013. **20**(7): p. 158.
20. Cambridge University Engineering Department, *Materials Data Book*. 2003. p. 11.
21. Stachurski, Z.H., *Strength and deformation of rigid polymers: the stress–strain curve in amorphous PMMA.* Polymer, 2003. **44**(19): p. 6067-6076.
22. Frazer, R.Q., et al., *PMMA: an essential material in medicine and dentistry.* Journal of long-term effects of medical implants, 2005. **15**(6).
23. Wong, D., et al., *Surface morphology and mechanical response of randomly oriented electrospun nanofibrous membrane.* Polymer Testing, 2016. **53**: p. 108-115.
24. Habiba, U., et al., *Adsorption and photocatalytic degradation of anionic dyes on Chitosan/PVA/Na–Titanate/TiO 2 composites synthesized by solution casting method.* Carbohydrate Polymers, 2016. **149**: p. 317-331.
25. Huang, Z.-M., et al., *Electrospinning and mechanical characterization of gelatin nanofibers.* Polymer, 2004. **45**(15): p. 5361-5368.
26. Tan, E.P.S., S.Y. Ng, and C.T. Lim, *Tensile testing of a single ultrafine polymeric fiber.* Biomaterials, 2005. **26**(13): p. 1453-1456.
27. Tan, E.P.S., et al., *Tensile test of a single nanofiber using an atomic force microscope tip.* Applied Physics Letters, 2005. **86**(7): p. 073115.
28. Hwang, K.Y., et al., *Mechanical characterization of nanofibers using a nanomanipulator and atomic force microscope cantilever in a scanning electron microscope.* Polymer Testing, 2010. **29**(3): p. 375-380.
29. Ridruejo, A., C. González, and J. Llorca, *Micromechanisms of deformation and fracture of polypropylene nonwoven fabrics.* International Journal of Solids and Structures, 2011. **48**(1): p. 153-162.
30. Jubera, R., et al., *Mechanical behavior and deformation micromechanisms of polypropylene nonwoven fabrics as a function of temperature and strain rate.* Mechanics of Materials, 2014. **74**: p. 14-25.
31. Lion, A., *A constitutive model for carbon black filled rubber: experimental investigations and mathematical representation.* Continuum Mechanics and Thermodynamics, 1996. **8**(3): p. 153-169.
32. Bergström, J. and M. Boyce, *Constitutive modeling of the large strain time-dependent behavior of elastomers.* Journal of the Mechanics and Physics of Solids, 1998. **46**(5): p. 931-954.
33. Rezakhaniha, R., et al., *Experimental investigation of collagen waviness and orientation in the arterial adventitia using confocal laser scanning microscopy.* Biomechanics and modeling in mechanobiology, 2012. **11**(3-4): p. 461-473.
34. Advani, S.G. and C.L. Tucker, *The Use of Tensors to Describe and Predict Fiber Orientation in Short Fiber Composites.* Journal of Rheology, 1987. **31**(8): p. 751-784.
35. Mohammad Khanlou, H., et al., *Electrospinning of polymethyl methacrylate nanofibers: optimization of processing parameters using the Taguchi design of experiments.* Textile Research Journal, 2015. **85**(4): p. 356-368.
36. Shenoy, S.L., et al., *Role of chain entanglements on fiber formation during electrospinning of polymer solutions: good solvent, non-specific polymer–polymer interaction limit.* Polymer, 2005. **46**(10): p. 3372-3384.
37. Deitzel, J.M., et al., *The effect of processing variables on the morphology of electrospun nanofibers and textiles.* Polymer, 2001. **42**(1): p. 261-272.
38. Fong, H., I. Chun, and D.H. Reneker, *Beaded nanofibers formed during electrospinning.* Polymer, 1999. **40**(16): p. 4585-4592.

39. Zong, X., et al., *Structure and process relationship of electrospun bioabsorbable nanofiber membranes.* Polymer, 2002. **43**(16): p. 4403-4412.
40. Li, D. and Y. Xia, *Electrospinning of nanofibers: reinventing the wheel?* Advanced materials, 2004. **16**(14): p. 1151-1170.
41. Zeleny, J., *The role of surface instability in electrical discharges from drops of alcohol and water in air at atmospheric pressure.* Journal of the Franklin Institute, 1935. **219**(6): p. 659-675.
42. Liu, Y., et al., *Preparation of novel ultrafine fibers based on DNA and poly(ethylene oxide) by electrospinning from aqueous solutions.* Reactive and Functional Polymers, 2007. **67**(5): p. 461-467.
43. Buchko, C.J., et al., *Processing and microstructural characterization of porous biocompatible protein polymer thin films.* Polymer, 1999. **40**(26): p. 7397-7407.
44. Shukla, S., et al., *Electrospinning of hydroxypropyl cellulose fibers and their application in synthesis of nano and submicron tin oxide fibers.* Polymer, 2005. **46**(26): p. 12130-12145.
45. Beyler, C.L. and M.M. Hirschler, *Thermal decomposition of polymers.* SFPE handbook of fire protection engineering, 2002. **2**.
46. Dixit, M., et al., *Morphology, miscibility and mechanical properties of PMMA/PC blends.* Phase Transitions, 2009. **82**(12): p. 866-878.
47. Callister, W.D. and D.G. Rethwisch, *Materials science and engineering: an introduction*. Vol. 7. 2007: Wiley New York.

Figures

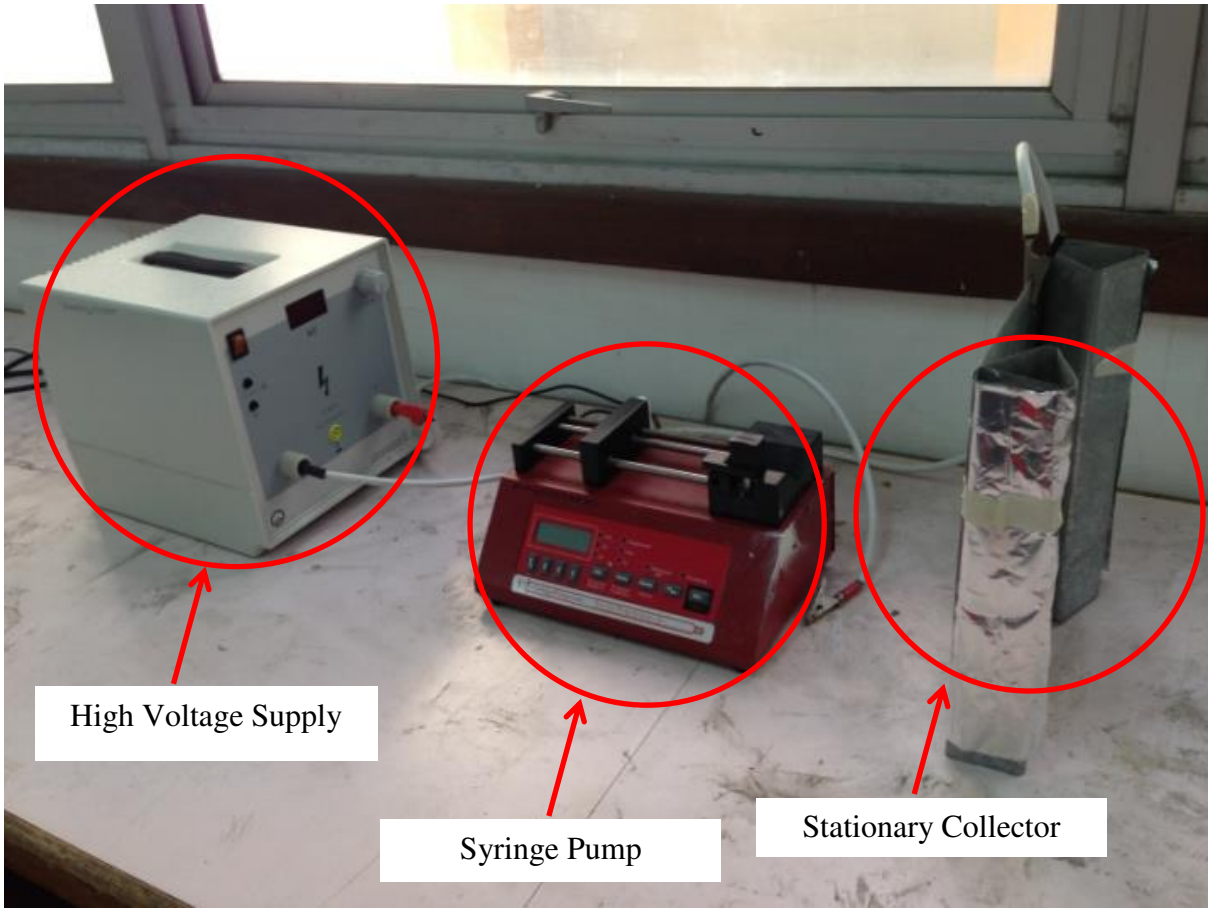

Figure 1. Setup for electrospinning.

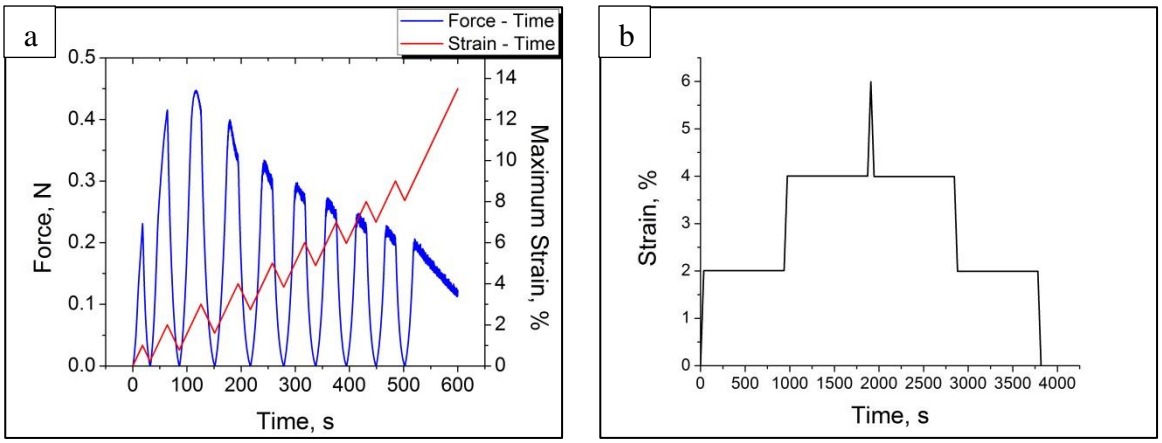

Figure 2. Loading profile for (a) cyclic loading test and (b) cyclic-relaxation test.

Figure 3. Red circle indicates the Deben tensile machine which is attached in SEM for in-situ tensile test.

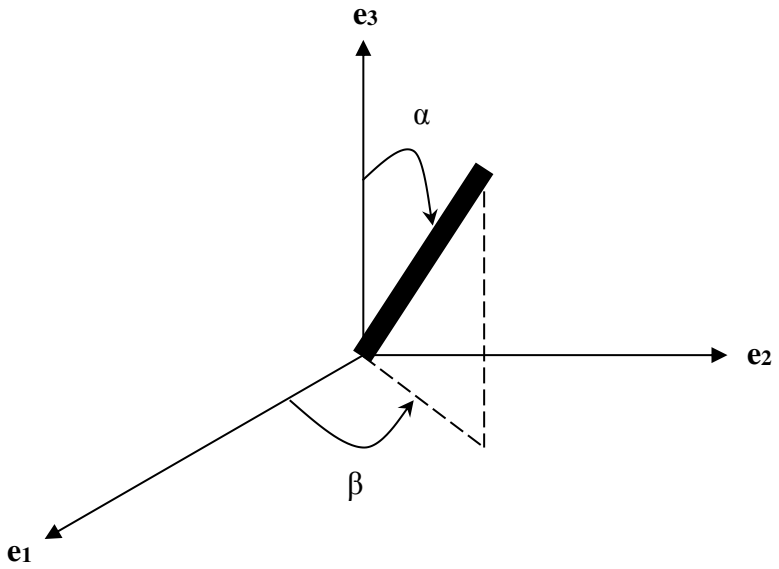

Figure 4. Characterization for an arbitrary unit direction vector **p** by means of Eulerian angles in a three-dimensional Cartesian coordinate system.

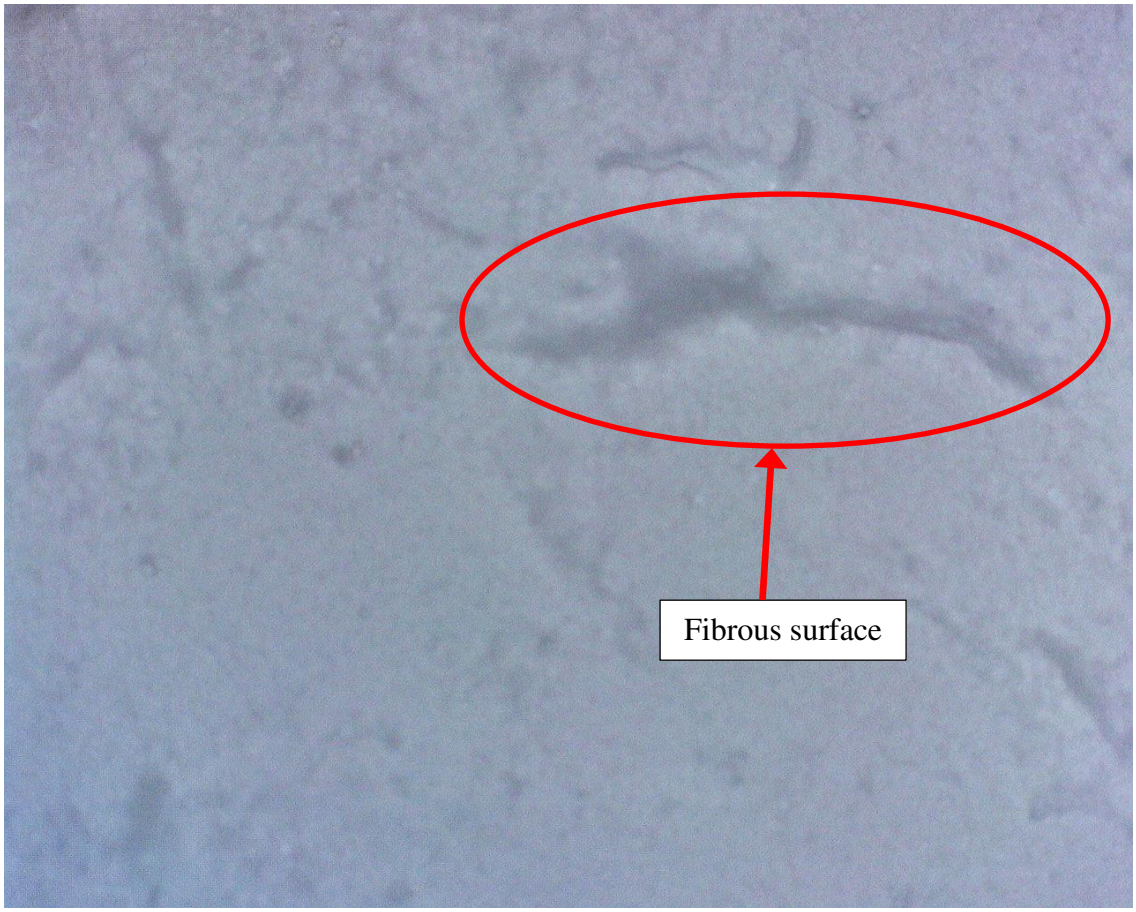

Figure 5. Image of electrospun low Mw PMMA nanofibrous membrane taken using digital microscope at 50x magnification.

Figure 6. Image of electrospun high Mw PMMA nanofibrous membrane taken using digital microscope at 50x magnification.

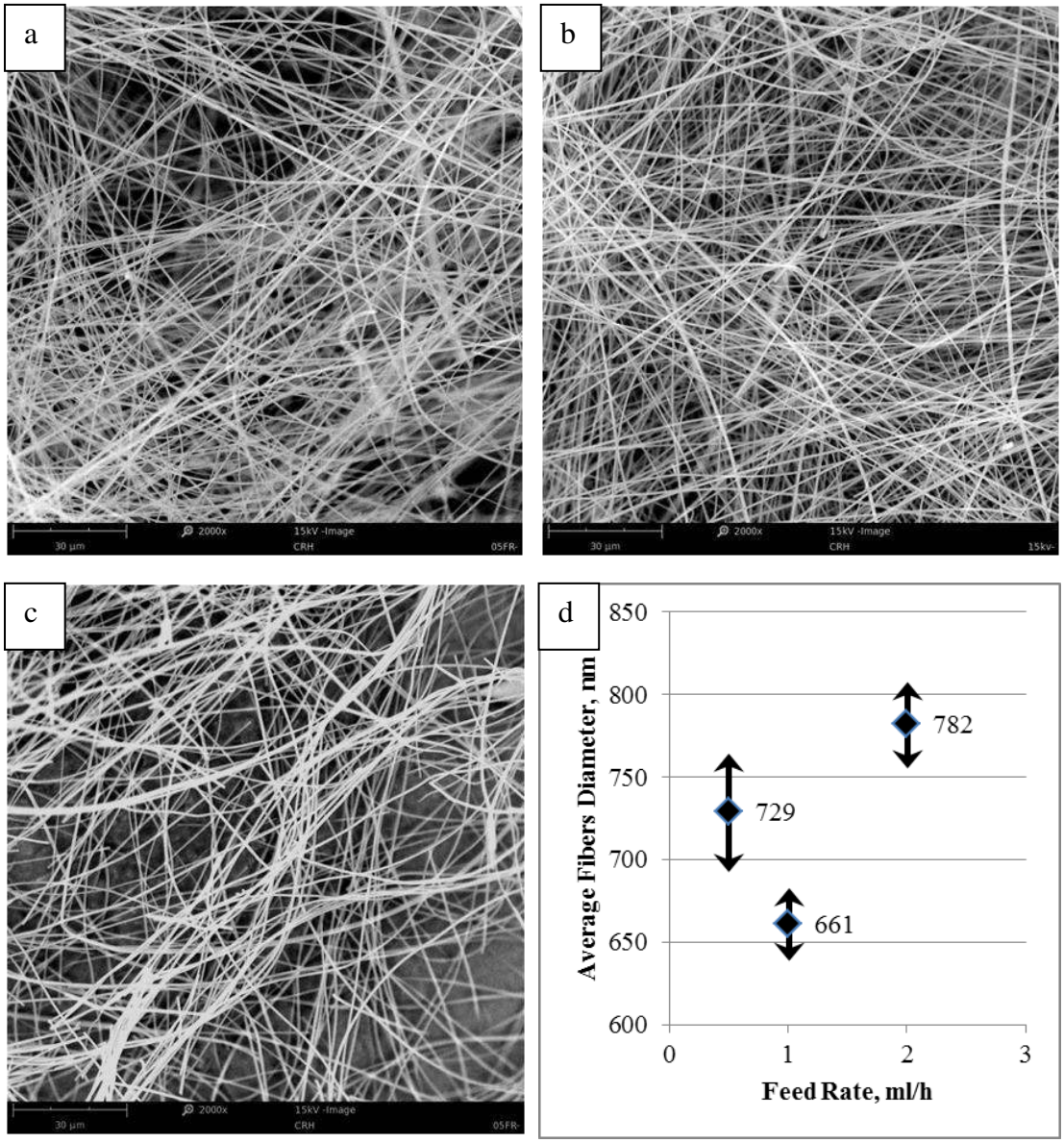

Figure 7. SEM images of Sample (a) F1, (b) F2, (c) F3 and (d) graph of average fiber diameter against feed rate.

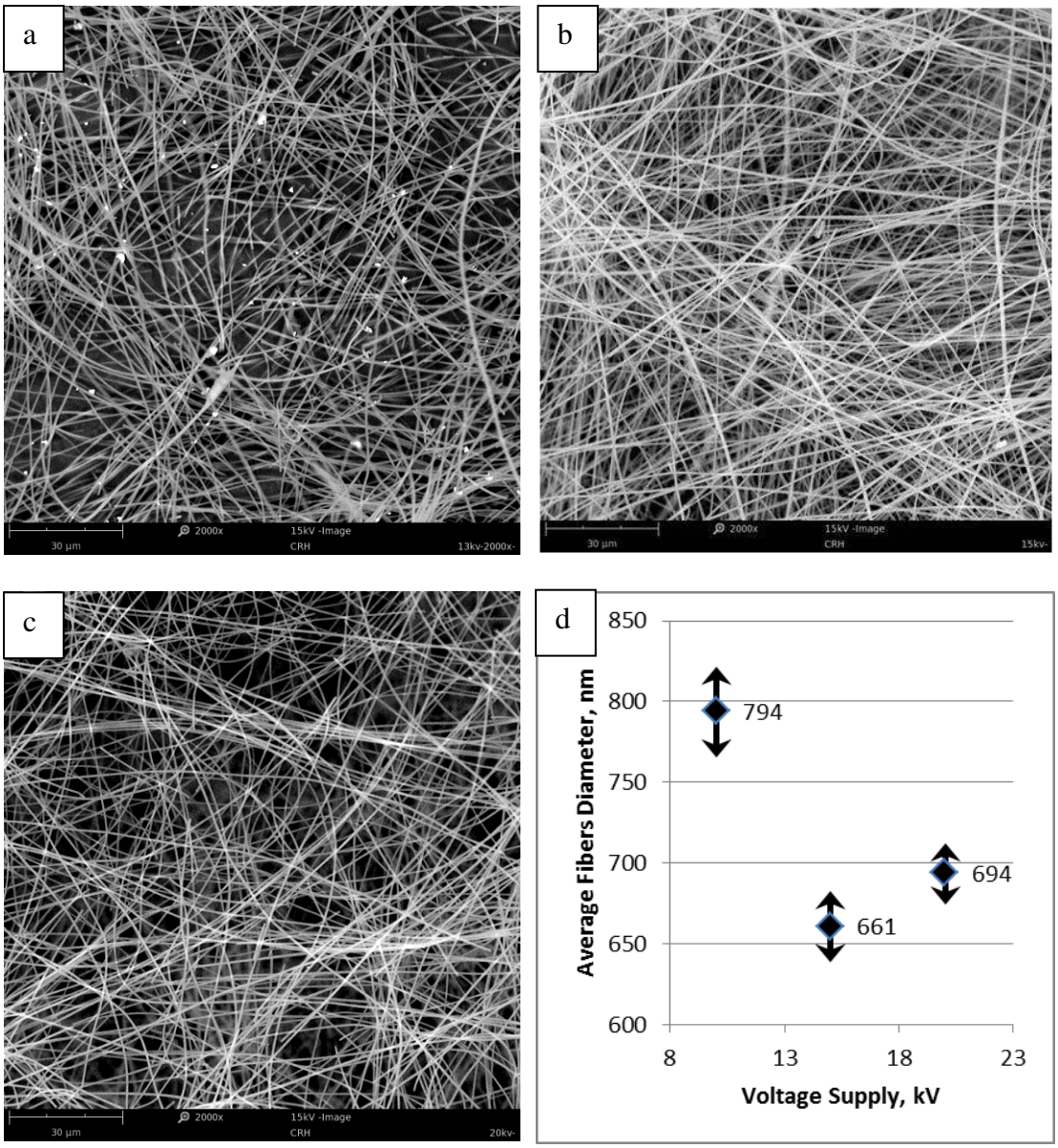

Figure 8. SEM images of Sample (a) V1, (b) F2 (c) V2 and (d) graph of average fibers diameter against supply voltage.

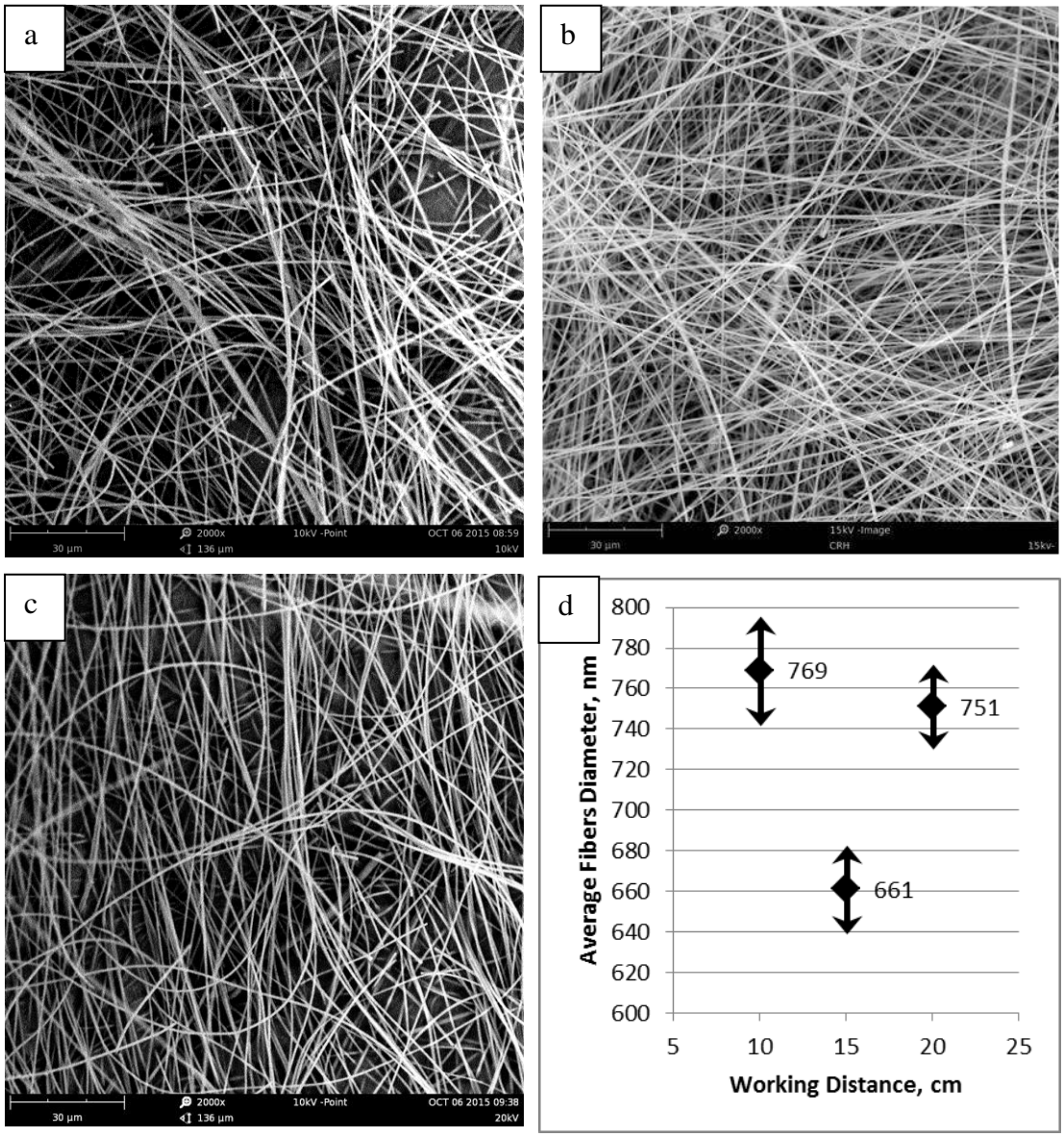

Figure 9. SEM images of Sample (a) D1, (b) F2 (c) D2 and (d) graph of average fibers diameter against working distance.

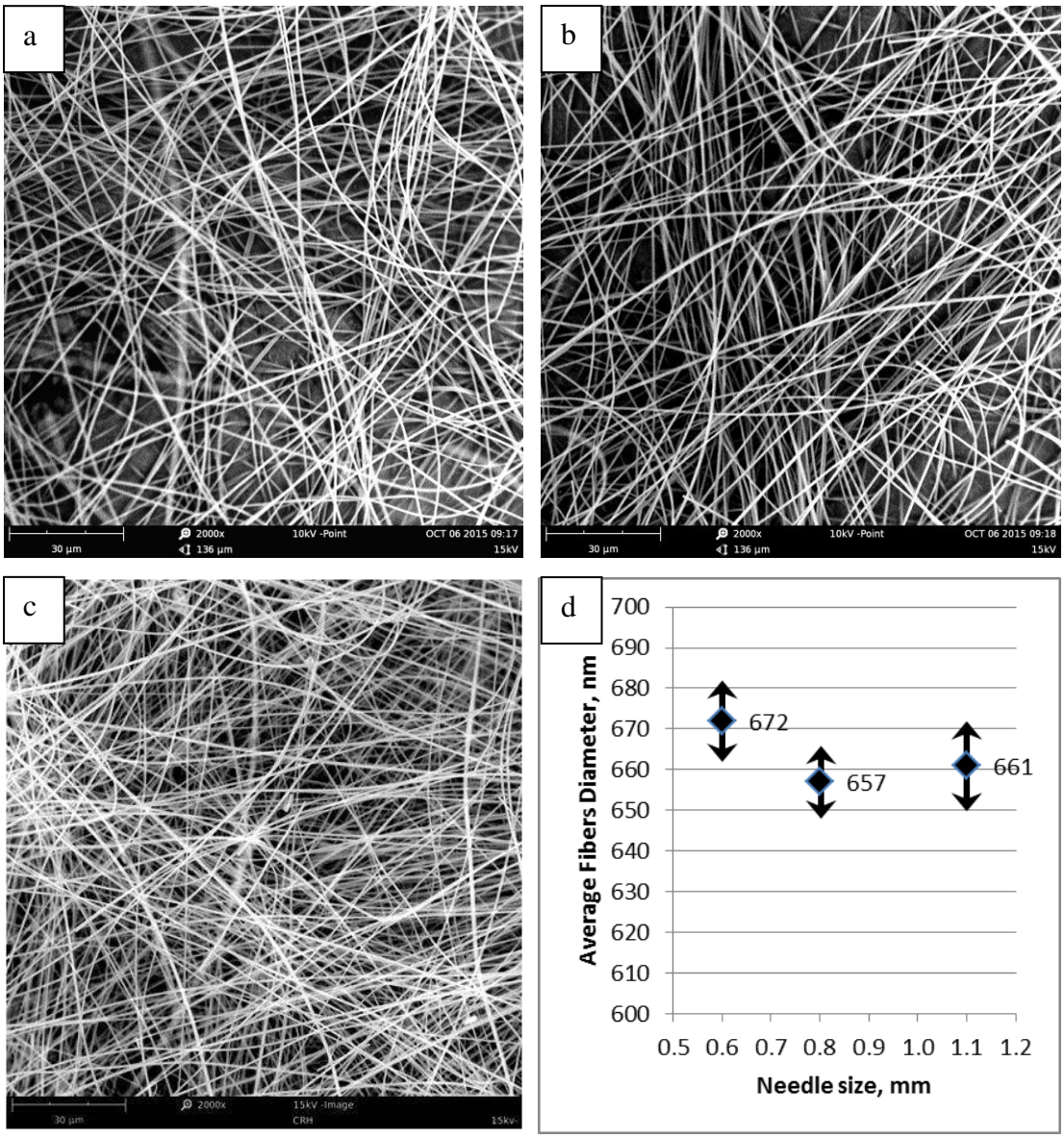

Figure 10. SEM images of Sample (a) G1, (b) G2 (c) F2 and (d) graph of average fibers diameter against gauge size.

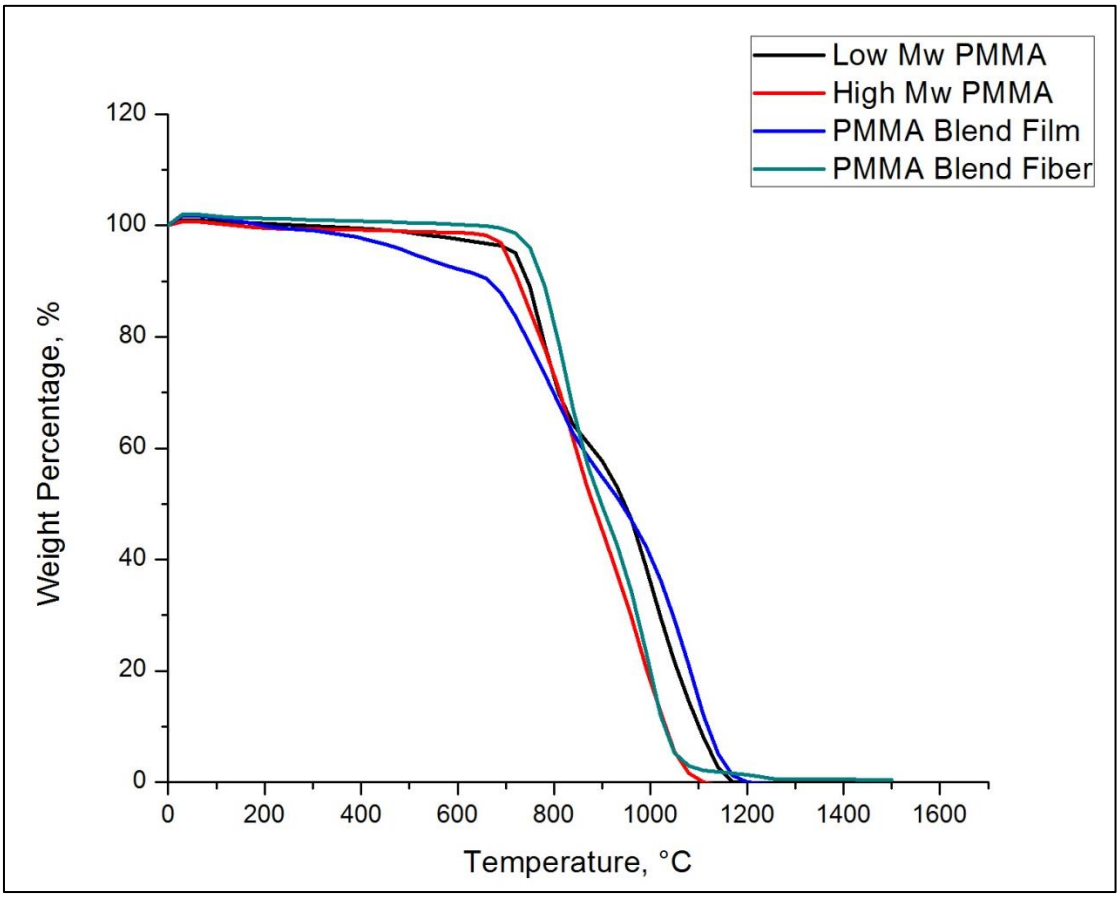

Figure 11. Graph of weight percentage against temperature obtained from TGA.

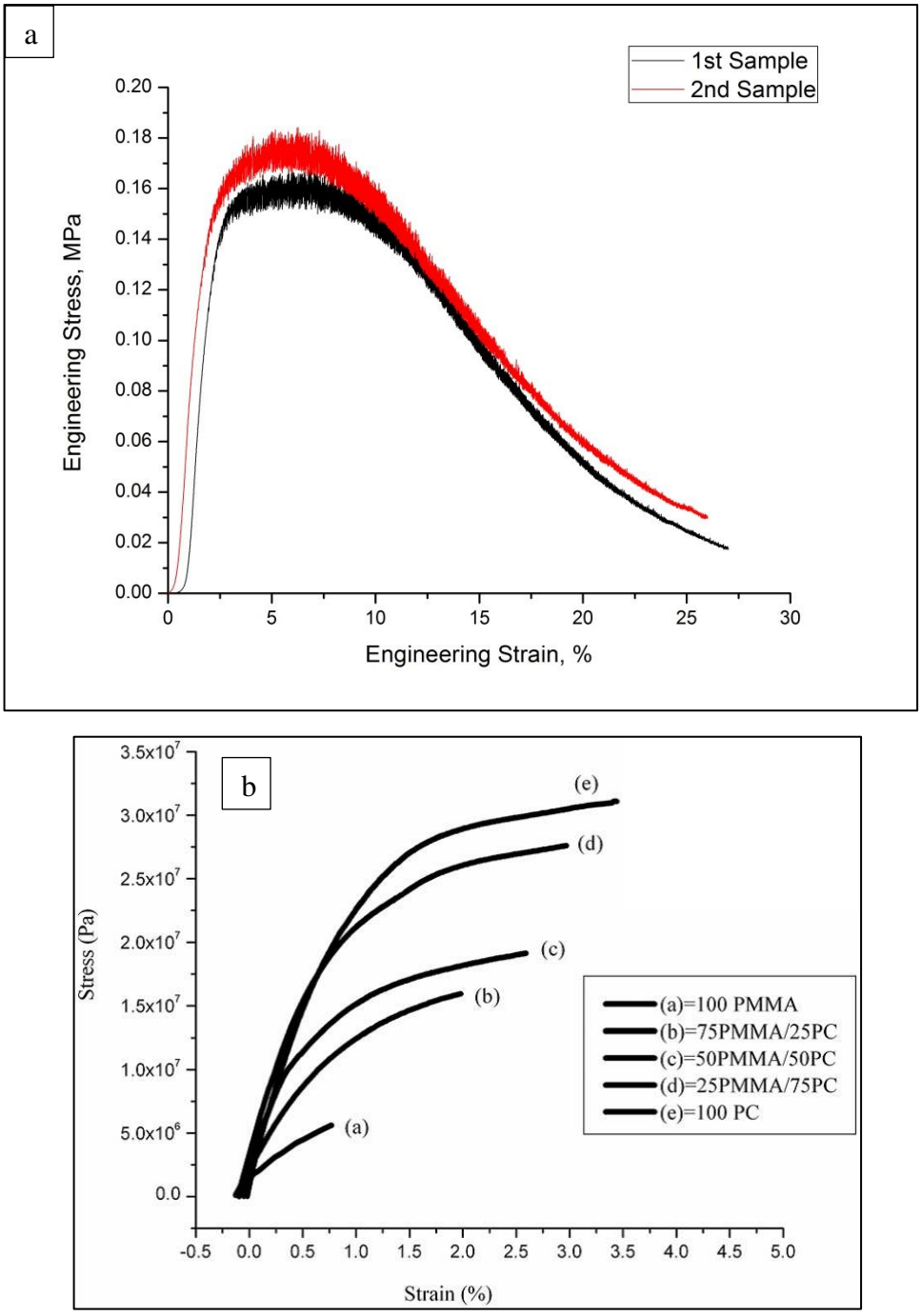

Figure 12. (a) Stress-strain curve of two samples at strain rate of 0.00055 sec^{-1} under monotonic tensile, (b) stress-strain curve of PMMA/PC film at different weight ratios [46]

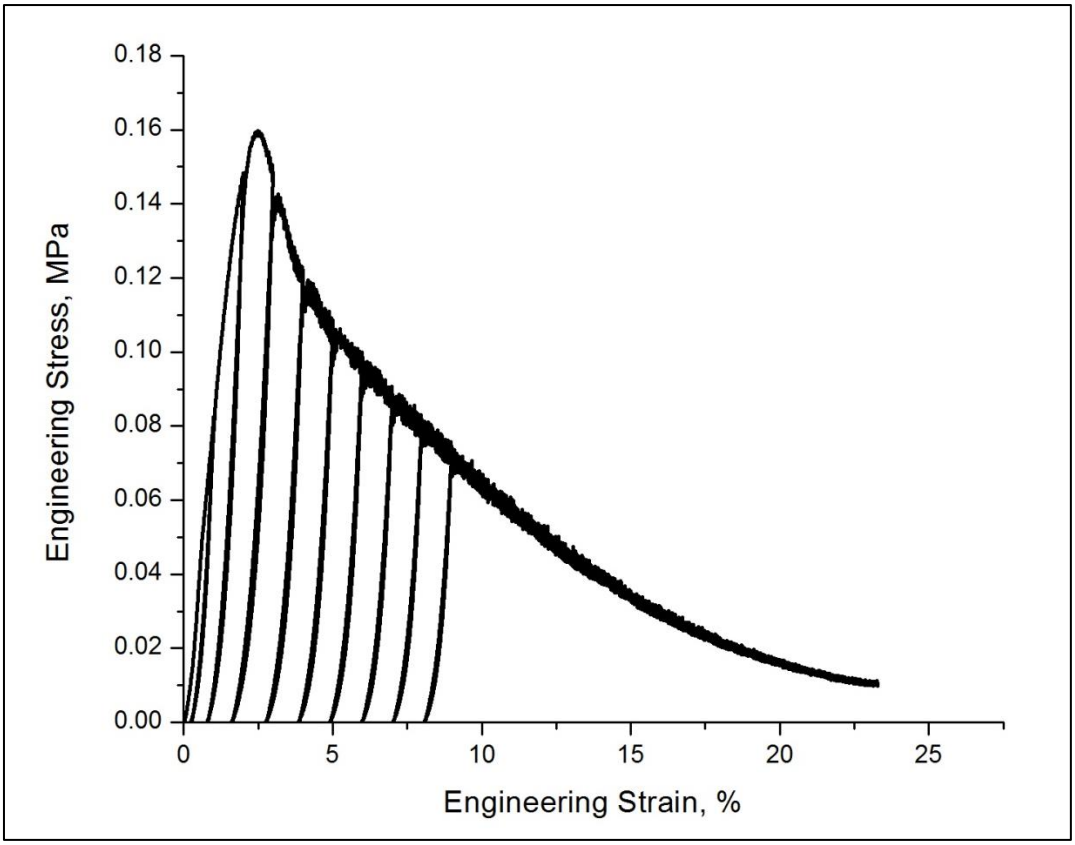

Figure 13. Stress-strain curve obtained from cyclic loading of Sample F2 at strain rate of 5.5×10^{-4} sec^{-1}.

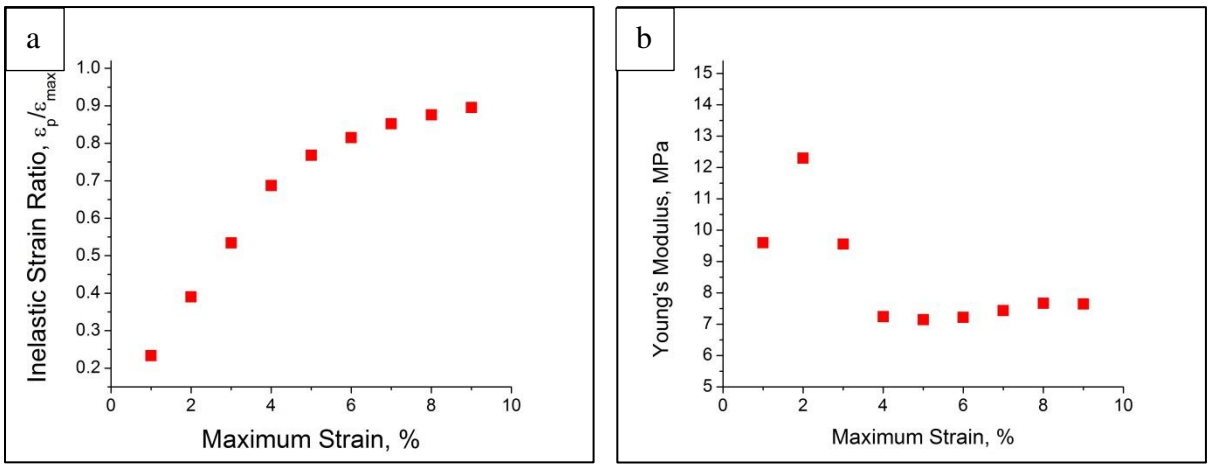

Figure 14. (a) Plot of inelastic strain ratio against maximum strain. (b) Plot of Young's Modulus versus maximum strain.

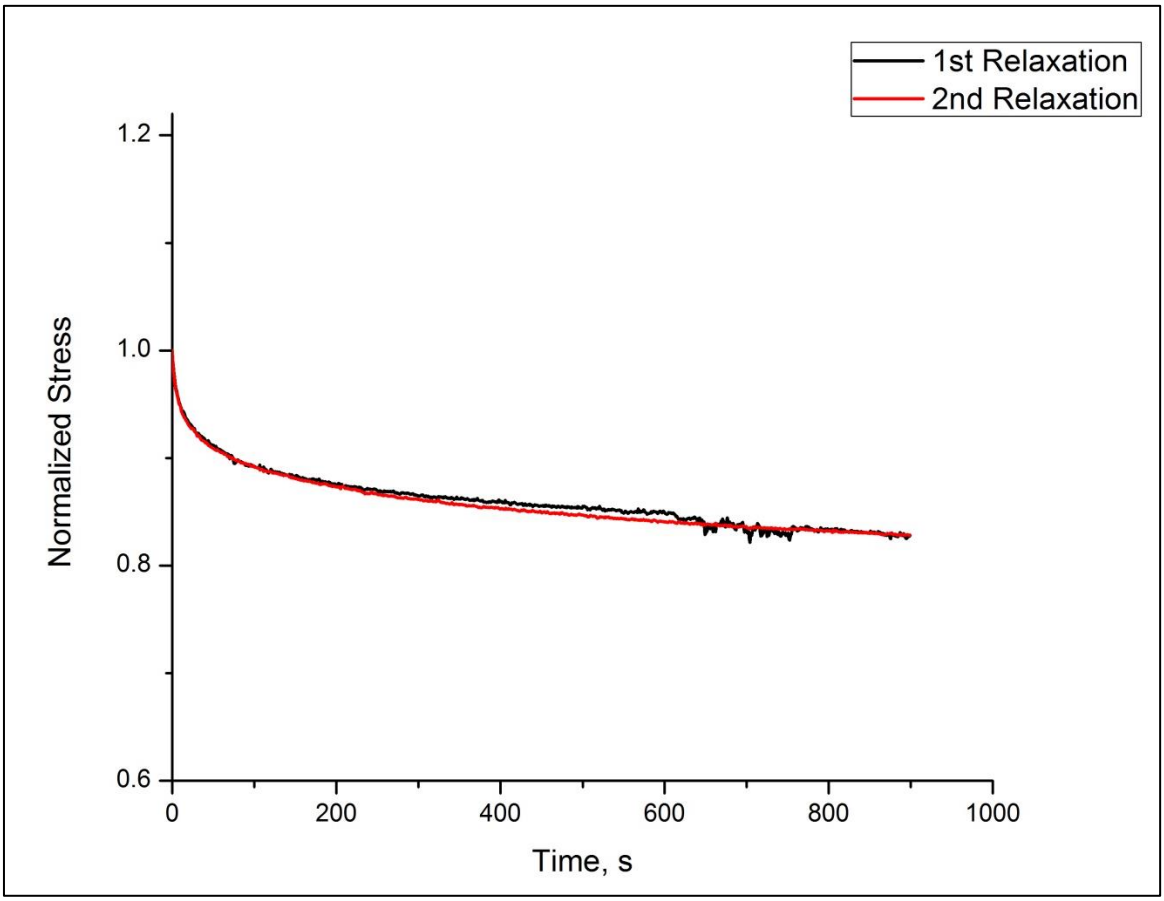

Figure 15. Plot of normalized stress for first relaxation and second relaxation against time.

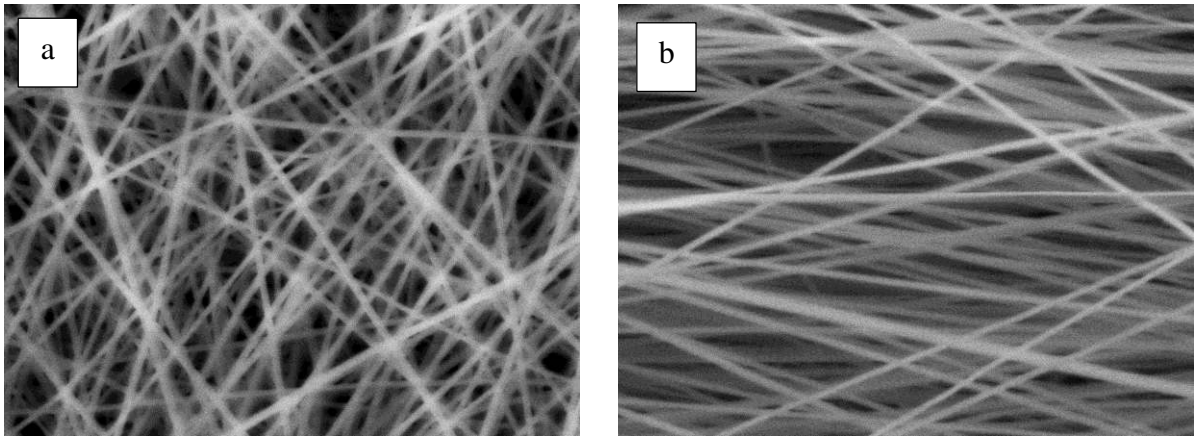

Figure 16. SEM images of nanofibrous membrane (a) before being stretched and (b) after being stretched to 30% engineering strain.

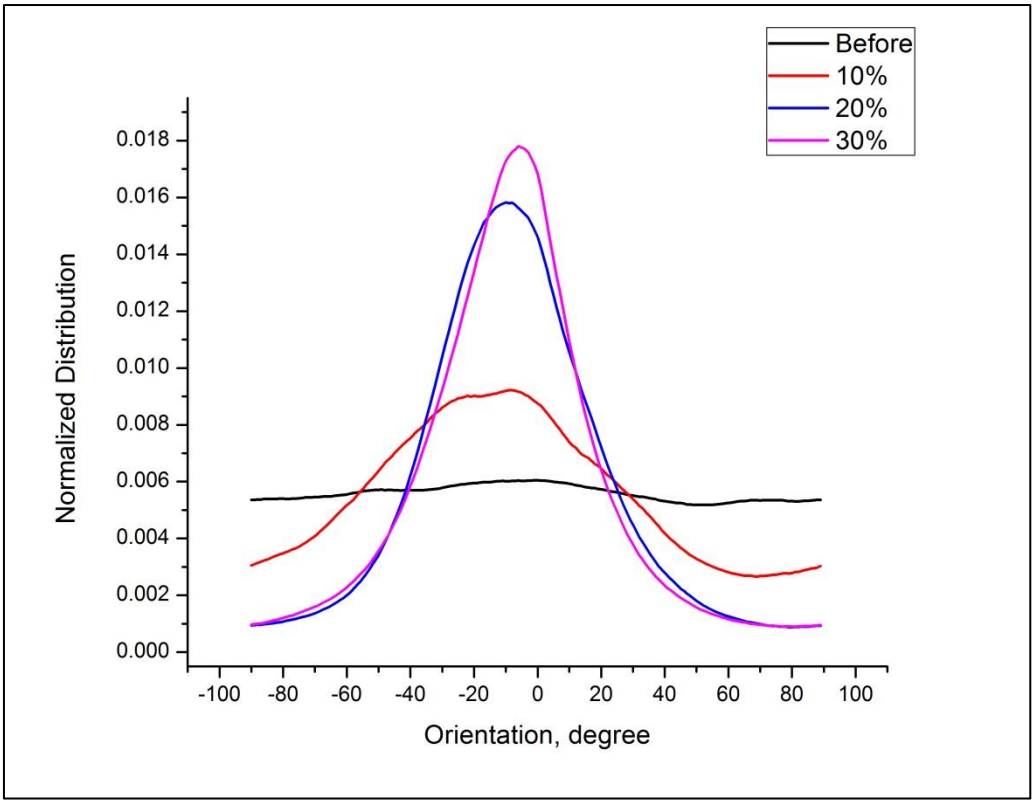

Figure 17. Graph of normalized distribution of fiber orientation against angle of fibers in nanofibrous membrane.

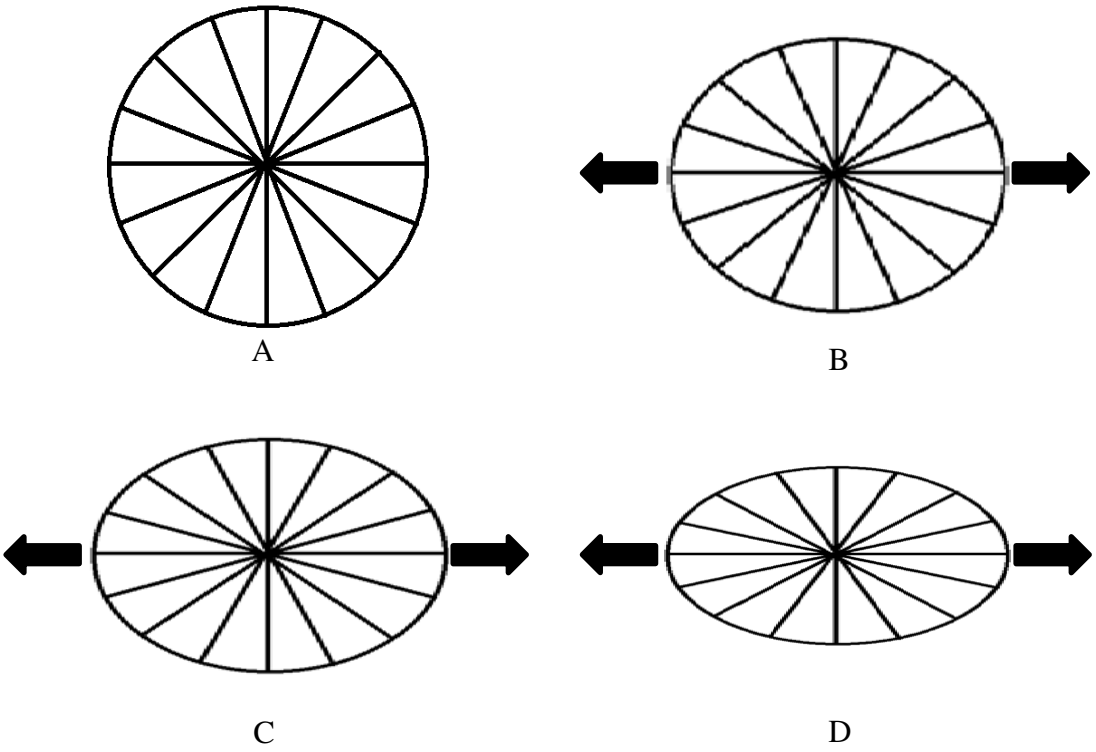

Figure 18. Illustrations of fibers orientation at strain levels A) 0 %, B) 10%, C) 20 % and D) 30 %.

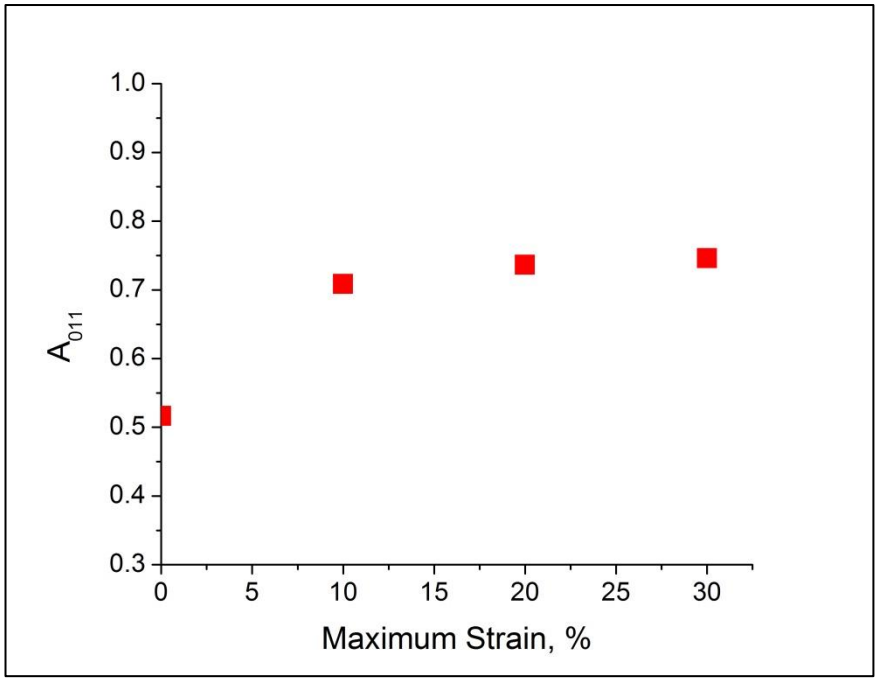

Figure 19. Graph of value of A_{011} against stretch of the nanofibrous membranes.

Tables

Table 1. List of samples with their respective electrospinning parameters.

Sample Reference	Wt% of high M_w PMMA	Wt% of low M_w PMMA	Feed rate, ml/h	Applied voltage, kV	Working distance, cm	Gauge size, mm	Electrospin-ability
H1	2	15	1.0	15	15	1.1	Yes
H2	3	15	1.0	15	15	1.1	Yes
H3	4	15	1.0	15	15	1.1	No
H4	5	15	1.0	15	15	1.1	No
P1	4	15	1.0	10	15	1.1	No
P2	4	15	1.0	20	15	1.1	No
P3	4	15	1.0	10	10	1.1	No
P4	4	15	1.0	20	20	1.1	No
P5	5	15	1.0	10	15	1.1	No
P6	5	15	1.0	20	15	1.1	No
P7	5	15	1.0	15	10	1.1	No
P8	5	15	1.0	15	20	1.1	No
P9	4	15	2.0	15	15	1.1	No
P10	5	15	2.0	15	15	1.1	No
A1	2	12	1.0	15	15	1.1	No
A2	3	12	1.0	15	15	1.1	No
A3	4	12	1.0	15	15	1.1	Yes
A4	5	12	1.0	15	15	1.1	Yes
B1	2	8	1.0	15	15	1.1	No
B2 (F2)	3	8	1.0	15	15	1.1	No
B3	4	8	1.0	15	15	1.1	Yes
B4	5	8	1.0	15	15	1.1	Yes
C1	2	20	1.0	15	15	1.1	Yes
C2	3	20	1.0	15	15	1.1	Yes
C3	4	20	1.0	15	15	1.1	No
C4	5	20	1.0	15	15	1.1	No
F1	4	8	0.5	15	15	1.1	Yes
F2 (B2)	4	8	1.0	15	15	1.1	Yes
F3	4	8	2.0	15	15	1.1	Yes
V1	4	8	1.0	10	15	1.1	Yes
V2	4	8	1.0	20	15	1.1	Yes
D1	4	8	1.0	15	10	1.1	Yes
D2	4	8	1.0	15	20	1.1	Yes